Progress In Electromagnetics Research, Vol. 117, 409–423, 2011

COUPLING MATRIX DECOMPOSITION IN DESIGNS AND APPLICATIONS OF MICROWAVE FILTERS

K. Xiao [1, *], L. F. Ye [1], F. Zhao [1], S. L. Chai [1], and L.-W. Li [2]

[1]College of Electronic Science and Engineering, National University of Defense Technology, Changsha 410073, China

[2]Institute of Electromagnetics, University of Electronic Science and Technology of China, Chengdu 611731, China

Abstract—The relationship between the immittance inverter coefficients and the coupling coefficients is obtained under the non-resonating coupling condition. With the relationship and the determinant properties of the transformation matrix, the coupling matrix could be decomposed to many sub-matrixes for filter designs. The physical significance of the decomposition is discussed. Using this idea, a filter can be decomposed to a number of sub-filters, which could be connected by sections of transmission lines with the same characteristics kept.

1. INTRODUCTION

Several techniques and methodologies are available nowadays for designing microwave filters with sharp cutoff at the edge of the passband. For some applications, such as space communication systems, it is desirable to sacrifice some signal to improve the close-to-band rejection slopes. A commonly adopted method used for achieving the high selectivity is to increase the degree of filters. Among some smart ideas used, transfer functions such as the elliptic function have been used to design filters with attenuation poles and sharp cutoff at the edge of the passband [1]. Multipath effects can be used to achieve transmission zeros [2], which depending on the phasing of the signal, may cause attenuation poles at finite frequencies. Multipath effects can be achieved by using cross coupling between

Received 26 April 2011, Accepted 9 June 2011, Scheduled 15 June 2011

* Corresponding author: Ke Xiao (xiaoke_e@hotmail.com).

modes in nonadjacent cavities [3–8]. After the multi-mode cavities are considered, multipath effects can be achieved by cross coupling between multi-mode cavities [9–12]. Bypass coupling is utilized to achieve the multipath effect [13–15], where the non-resonating (NRN) modes were used to realize the bypass coupling, although NRN is not proper for wideband design since the resonance of the NRN can not be allocated far from the passband, it is also a disadvantage of the use of NRN that the design produce longer filters but not increase the filter order or selectivity [7].

A matrix decomposition method in this paper is proposed to design high-order filters. The idea is to divide the coupling between two resonators into two NRN coupling, so that some large coupling values can be made more physically realizable. From the determinant properties of transformation matrix and the expressions of the filter response getting from the coupling matrix, the high-degree coupling matrix can be mathematically divided into a number of sub-matrices (which are associated with NRN coupling). So, the original proposed high-degree filter can be physically decomposed to sub-filters which can be designed separately and individually.

2. INVERTER AND COUPLING NETWORKS

Three cases are usually considered to analyze the relationships between immittance inverter coefficients and coupling coefficients, namely,

(1) Coupling between resonating modes,

(2) Coupling between resonating and NRN modes,

(3) Coupling between NRN modes.

The relationship in Case 2 was analyzed by means of external quality factor [13, 16], where Amari designed the filter using the coupling between the NRN $TE_{10/01}$ modes and source/load as the bypass coupling, then the bypass coupling effects can be described by coupling matrix. As the relationship in Case 1 is very similar to that in Case 3, so we will only address the issues in Case 3 herein.

The NRN modes are defined as these modes whose resonating frequencies are far away from their pass bandwidths of the respective filters. Within the bandpass of filters, the coupling between NRN modes is equivalent to the transmission line coupling, and the presumed NRN modes become equivalent to transmission loads. So, we consider a two-port network comprising of the NRN coupling circuits as shown in Fig. 1(a), two sections (characterized by $\{G_1, \phi_1\}$) and $\{G_2, \phi_2\}$) of transmission lines are added to the two sides (denoted by A and B) of the immittance inverter.

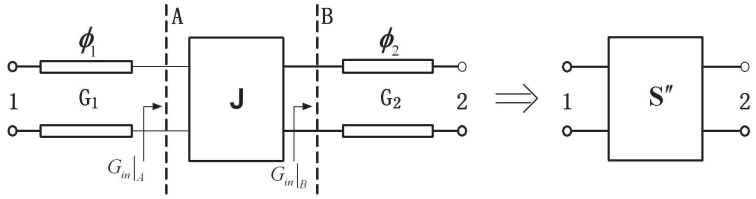

Figure 1. Layout of admittance inverter network. (a) Immittance inverter with two transmission lines. (b) Equivalent two-port network.

In Fig. 1(a), the two parameters, G_1 and G_2, represent the characteristic admittances of the two NRN transmission lines while the other two, ϕ_1 and ϕ_2, denote the related phase-shifts of the transmission lines, respectively. The scattering parameters of the two-port network shown in Fig. 1(b) can be calculated as follows:

$$S''_{11} = \frac{(G_1G_2)/J^2 - 1}{(G_1G_2)/J^2 + 1} e^{-2j\phi_1} = \left|S''_{11}\right| e^{j\theta''_{S_{11}}} \tag{1}$$

where $\theta''_{S_{11}}$ denotes the phase of S''_{11}. In a similar fashion to the S-parameter in (1), another expression can be obtained for the S-parameter S''_{22}. From (1), we have:
for $\dfrac{G_1G_2}{J^2} < 1$

$$\left|S''_{11}\right| = \left|S''_{22}\right| = \frac{1 - (G_1G_2)/J^2}{1 + (G_1G_2)/J^2}, \tag{2}$$

$$\phi_i = -\frac{1}{2}\theta''_{S_{ii}} + \frac{(2m+1)}{2}\pi \tag{3}$$

where $i = 1, 2$, and $m \in \mathcal{Z}$; while for $\dfrac{G_1G_2}{J^2} > 1$

$$\left|S''_{11}\right| = \left|S''_{22}\right| = \frac{(G_1G_2)/J^2 - 1}{(G_1G_2)/J^2 + 1}, \tag{4}$$

$$\phi_i = -\frac{1}{2}\theta''_{S_{ii}} + n\pi, \text{ where } n \in \mathcal{Z}. \tag{5}$$

To obtain the scattering characteristics of the network without the phase-shift-segment, we set $\phi_1 = \phi_2 = 0$ for the two cases, yielding

$$\left.\begin{array}{l} \theta''_{S_{11}} = (2p+1)\,\pi \\ \theta''_{S_{22}} = (2q+1)\,\pi \end{array}\right\}, \text{ where } \{p,\, q\} \in \mathcal{Z}, \tag{6}$$

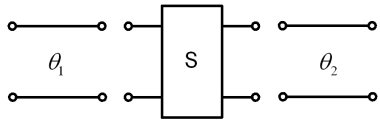

Figure 2. Geometry of cascaded two-port networks.

$$\left.\begin{array}{l}\theta''_{S_{11}} = 2t\pi \\ \theta''_{S_{22}} = 2s\pi\end{array}\right\}, \text{ where } \{t,\, s\} \in \mathcal{Z}. \tag{7}$$

Both of two cases are possible, the scattering parameters of the admittance inverter are derived, then in order to yield the equivalent relation between the admittance inverter coefficient and the coupling coefficient, we need to know the scattering parameters of the coupling network, so we consider a two-port network shown in Fig. 2.

Define the coupling between the non-resonators characterized by the coefficient M_{SL} [13]. According to the relationship between the filter's response and coupling matrix, we have

$$M_{SL} = \frac{jS_{21}}{1 - S_{11}}, \tag{8}$$

where S_{21} and S_{11} are the scattering parameters of the two-port network S in Fig. 2. As the coupling parameter M_{SL} defined in (8) is a complex number, the phase shift section is added in each side in order to obtain a real part of M_{SL}. Define the cascaded networks as S' in Fig. 2. The scattering parameter of S' in Fig. 2 can be expressed as

$$S' = \begin{bmatrix} e^{-j2\theta_1} S_{11} & e^{-j\theta_1} e^{-j\theta_2} S_{12} \\ e^{-j\theta_1} e^{-j\theta_2} S_{21} & e^{-j2\theta_2} S_{22} \end{bmatrix}. \tag{9}$$

The coupling coefficient M'_{SL} after cascading becomes

$$M'_{SL} = \frac{S'_{21}}{j\left(S'_{11} - 1\right)} = \frac{e^{-j\left(\theta_1 + \theta_2 - \theta_{21} - \frac{\pi}{2}\right)} \left|S_{21}\right|}{1 - e^{-j(2\theta_1 - \theta_{11})} \left|S_{11}\right|} \tag{10}$$

where θ_{11} and θ_{21} denote the phases of S_{11} and S_{21} respectively, while $|S'_{11}|$ and $|S'_{21}|$ stand for the scattering parameters after cascading. To obtain a real value of M'_{SL}, we have

$$\theta_1 + \theta_2 - \theta_{21} + \frac{\pi}{2} = p\pi, \quad p \in \mathcal{Z}, \tag{11}$$

$$\theta_1 - \theta_{11} = q\pi, \quad q \in \mathcal{Z}. \tag{12}$$

Assuming that all the network systems analyzed and considered are lossless and of reciprocity, we then have

$$\theta_{21} = \theta_{12} = \frac{1}{2}\left(\theta_{11} + \theta_{22} - \pi\right). \tag{13}$$

Substituting (13) into (11) and (12) yields

$$\left.\begin{aligned}\theta_1 &= \frac{\theta_{11}}{2} + \frac{n\pi}{2} \\ \theta_2 &= \frac{\theta_{22}}{2} + \frac{m\pi}{2}\end{aligned}\right\}, \text{ where } \{n, m\} \in \mathcal{Z}. \tag{14}$$

With the phase condition given in (14), two sets of coupling coefficients can be obtained. The first set of coefficients is given by

$$M'_{SL1} = \frac{\pm|S_{21}|}{1+|S_{11}|} = \frac{\pm|S'_{21}|}{1+|S'_{11}|} \tag{15}$$

$$\left.\begin{aligned}\theta_1 &= \frac{\theta_{11}}{2} + \frac{(2n+1)\,\pi}{2} \\ \theta_2 &= \frac{\theta_{22}}{2} + \frac{(2m+1)\,\pi}{2}\end{aligned}\right\}, \text{ where } \{n, m\} \in \mathcal{Z}, \tag{16}$$

$$\left.\begin{aligned}\theta_{S'_{11}} &= (2e+1)\,\pi \\ \theta_{S'_{22}} &= (2f+1)\,\pi\end{aligned}\right\}, \text{ where } \{e, f\} \in \mathcal{Z}. \tag{17}$$

The second set of coefficients is expressed as

$$M'_{SL2} = \frac{\pm|S_{21}|}{1-|S_{11}|} = \frac{\pm|S'_{21}|}{1-|S'_{11}|} \tag{18}$$

$$\left.\begin{aligned}\theta_1 &= \frac{\theta_{11}}{2} + n\pi \\ \theta_2 &= \frac{\theta_{22}}{2} + m\pi\end{aligned}\right\}, \text{ where } \{n, m\} \in \mathcal{Z}, \tag{19}$$

$$\left.\begin{aligned}\theta_{S'_{11}} &= 2e\pi \\ \theta_{S'_{22}} &= 2f\pi\end{aligned}\right\}, \text{ where } \{e, f\} \in \mathcal{Z} \tag{20}$$

where S'_{11} and S'_{22} denote the scattering parameters of the network S', while $\theta_{S'_{11}}$ and $\theta_{S'_{22}}$ stand for the phases of S'_{11} and S'_{22}, respectively.

The phase conditions defined in (6) and (17) are found to be equivalent. And by comparing the scattering parameters given by (2), (3) and (6) versus (15), (16) and (17), the relation between the coupling and the admittance inverter coefficients can be derived as

$$M'_{SL} = \frac{\sqrt{G_1 G_2}}{J} = \frac{\pm|S''_{21}|}{1+|S''_{11}|} = \frac{\pm|S'_{21}|}{1+|S'_{11}|}. \tag{21}$$

Using the same method, the phase conditions of (7) and (20) are also found to be equivalent. And using (4), (5) and (7) versus (18), (19) and (20), we obtain another relation expressed as

$$M'_{SL} = \frac{J}{\sqrt{G_1 G_2}} = \frac{\pm|S_{21}|}{1-|S_{11}|} = \frac{\pm|S'_{21}|}{1-|S'_{11}|}. \tag{22}$$

The methods proposed above can be used to obtain similar relations for the impedance inverter coefficients and the coupling coefficients.

3. COUPLING DECOMPOSITION SCHEME

Considering the admittance inverters on the left-hand side of Fig. 3, we have $J = -(J_1 J_3)/J_2$. On the right-hand side of Fig. 3, the inverter coefficients of three cascaded admittance inverters are J_1, J_2 and J_3, respectively, and G_1, G_2, G_3 and G_4 represent characteristic admittances of the transmission lines connected. The transfer matrices of the two networks shown in Fig. 3 are equivalent.

From (22), coupling coefficients corresponding to the four inverter networks are expressed as $M = -J/\sqrt{G_1 G_4}$, $M_1 = J_1/\sqrt{G_1 G_2}$, $M_2 = J_2/\sqrt{G_2 G_3}$, and $M_3 = J/\sqrt{G_3 G_4}$, respectively. They are found to satisfy the equation $M = -(M_1 M_3)/M_2$. By using the equation, the coupling coefficients can be decomposed, e.g., when $M_2 = 1$, $M = -M_1 M_3$. Considering the coupling matrix $\bar{B}$ in (23) and using the determinant transforming, we have a coupling matrix $\bar{A}$ as shown in (24) with the same filter response of $\bar{B}$ [13, 16].

$$\bar{B} = \begin{bmatrix} -j & M_{12} & \cdots & M_{1,i} & & \\ M_{12} & p & \cdots & \vdots & & \\ \vdots & \vdots & \ddots & M_{i-1,i} & & \\ M_{1,i} & \cdots & M_{i-1,i} & p & & \\ M_{1,i+1} & \cdots & M_{i-1,i+1} & -M_{i,i+1}M'_{i,i+1} & & \\ M_{1,i+2} & \vdots & \vdots & M_{i,i+2} & & \\ \vdots & \vdots & \vdots & \vdots & & \\ M_{1,N+2} & \cdots & \cdots & \cdots & & \end{bmatrix} \begin{bmatrix} M_{1,i+1} & M_{1,i+2} & \cdots & M_{1,N+2} \\ \vdots & \vdots & \cdots & \vdots \\ M_{i-1,i+1} & \vdots & \cdots & \vdots \\ -M_{i,i+1}M'_{i,i+1} & M_{i,i+2} & \cdots & M_{i,N+2} \\ p & M_{i+1,i+2} & \cdots & M_{i+1,N+2} \\ M_{i+1,i+2} & \ddots & \vdots & \vdots \\ \vdots & \cdots & p & M_{N+1,N+2} \\ M_{i+1,N+2} & \cdots & M_{N+1,N+2} & -j \end{bmatrix} \tag{23}$$

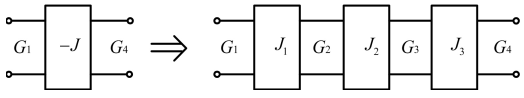

Figure 3. Two equivalent admittance inverter networks.

In which, p means the complex lowpass frequency variable, expressed as $p = j\left(\omega/\omega_0 - \omega_0/\omega\right)/FBW$, where $FBW = \Delta\omega/\omega_0$ is the fractional bandwidth of filter [16].

$$\bar{A} = \begin{bmatrix} -j & M_{12} & \cdots & M_{1,i} & 0 \\ M_{12} & p & \cdots & \vdots & \vdots \\ \vdots & \vdots & \ddots & M_{i-1,i} & 0 \\ M_{1,i} & \cdots & M_{i-1,i} & p & M_{i,i+1} \\ 0 & \cdots & 0 & M_{i,i+1} & 0 \\ 0 & \cdots & 0 & 0 & 1 \\ M_{1,i+1} & \cdots & M_{i-1,i+1} & 0 & 0 \\ M_{1,i+2} & \cdots & \cdots & M_{i,i+2} & 0 \\ \vdots & \vdots & \vdots & \vdots & \vdots \\ M_{1,N+2} & \cdots & \cdots & M_{i,N+2} & 0 \end{bmatrix}$$

$$\begin{bmatrix} 0 & M_{1,i+1} & M_{1,i+2} & \cdots & M_{1,N+2} \\ \vdots & \vdots & \vdots & \cdots & \vdots \\ 0 & M_{i-1,i+1} & \vdots & \cdots & \vdots \\ 0 & 0 & M_{i,i+2} & \cdots & M_{i,N+2} \\ 1 & 0 & 0 & \cdots & 0 \\ 0 & M'_{i,i+1} & 0 & \cdots & 0 \\ M'_{i,i+1} & p & M_{i+1,i+2} & \cdots & M_{i+1,N+2} \\ 0 & M_{i+1,i+2} & \ddots & \vdots & \vdots \\ \vdots & \vdots & \vdots & p & M_{N+1,N+2} \\ 0 & M_{i+1,N+2} & \cdots & M_{N+1,N+2} & -j \end{bmatrix} \tag{24}$$

From the determinant transforming, we obtain $\left|\bar{A}\right| = -\left|\bar{B}\right|$ and $\bar{A}^*_{N+2,1} = -\bar{B}^*_{N,1}$, in which, $\bar{A}^*_{ij}$ means the cofactor of the element a_{ij}. Equations used to calculate the transmission and reflection coefficients (or scattering parameters) of the filters from the coupling matrix $\bar{A}$ or $\bar{B}$ are given as follows

$$S_{11} = 1 - 2R_S I_1 = 1 + 2j\left[\bar{A}^{-1}\right]_{11} \tag{25}$$

$$S_{21} = 2\sqrt{R_S R_L} I_n = -2j\left[\bar{A}^{-1}\right]_{n1} \tag{26}$$

where

$$\left[\bar{A}^{-1}\right]_{n1} = \frac{1}{\left|\bar{A}\right|}\bar{A}^*_{n1}. \tag{27}$$

From (25), (26) and (27), the ideal filter responses corresponding to coupling matrices $\bar{A}$ and $\bar{B}$ are equivalent. Especially when $M_{n,i+1} = 0$ $(1 \le n \le i-1)$ and $M_{i,m} = 0$ $(i+2 \le m \le N+2)$ in the coupling matrix

$\bar{B}$, the response of matrix $\bar{A}$ will have independent transmission zeros between sub-matrices, which will be demonstrated in the following examples.

4. NRN COUPLING OF MATCHING NETWORKS

In Fig. 4, the impedance inverter coefficient of the network highlighted by the elliptical circular is Z_C, and the characteristic impedance of the transmission lines with phase-shifts of ϕ_1 and ϕ_2 is also Z_C.

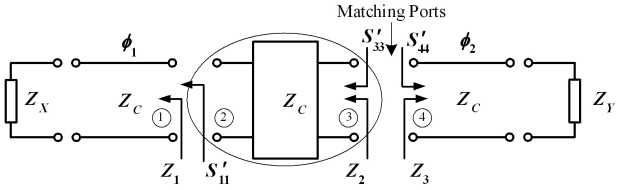

Figure 4. NRN coupling between two networks.

From equations obtained in Section 2, the coupling coefficient of the inverter network is equal to 1, so the inverter of "Z_C" can be replaced by a section of $\lambda_g/4$ transmission line whose characteristic impedance is also Z_C. In Fig. 4, Z_X and Z_Y represent the equivalent loads to sub-filter circuits, while Z_X and Z_Y denote actually complex impedances dependant upon the frequency. In the pass-band of the filter, Z_X and Z_Y trend to Z_C. The input impedances of the ports indicated in Fig. 4 are expressed as

$$Z_1 = Z_C \frac{Z_X + jZ_C \tan\phi_1}{Z_C + jZ_X \tan\phi_1}, \tag{28}$$

$$Z_3 = Z_C \frac{Z_Y + jZ_C \tan\phi_2}{Z_C + jZ_Y \tan\phi_2}, \tag{29}$$

$$Z_2 = Z_C \frac{Z_C + jZ_X \tan\phi_1}{Z_X + jZ_C \tan\phi_1} = Z_C \frac{Z_X + jZ_C \tan(\phi_1 + \pi/2)}{Z_C + jZ_X \tan(\phi_1 + \pi/2)} \tag{30}$$

Consider the matching of Ports 3 and 4. As the conjugate matching is obtained exactly in pass-band, namely, $Z_2 = \bar{Z}_3$, so a non-linear relation between ϕ_1 and ϕ_2 can be deduced. The general expression of the relation is very complicated, so it is impractical to express it explicitly herewith. We could consider, however, a simplified case at first, that is, a symmetry filter of even degree whose NRN coupling part is just located in the symmetric position.

Due to the symmetry assumed, so $Z_X = Z_Y$ and $\phi_1 = \phi_2$ can be obtained. Therefore, we have $Z_1 = Z_3$. As mentioned earlier, the "1"

coupling section can be equivalent to a section of $\lambda_g/4$ transmission line, so the phase difference between the reflection coefficients S'_{33} and S'_{44} is π. From the conjugate matching condition $Z_2 = \bar{Z}_3$, we should obtain $S'_{33} = \bar{S}'_{44}$, which means at a frequency, f and within its pass-band, the reflection coefficients $S'_{33}(f)$ and $S'_{44}(f)$ should be symmetrical with respect to the real axis on the Smith Chart. Together with the phase difference condition of $S'_{33}(f)$ and $S'_{44}(f)$, the ideal conjugate matching implies that by choosing a proper ϕ_1 [or ϕ_2 for instance], the track of reflection coefficient $S'_{33}(f)$ [or $S'_{44}(f)$] within the frequency pass-band should be perpendicular to the real axis and should pass through the Smith Chart center. It is, however, impossible to find such a linear relation of ϕ_1 to satisfy this ideal condition due to the frequency dependence. Only an approximate matching condition can be used by tuning ϕ_1 to match the track of $S'_{33}(f)$ [or $S'_{44}(f)$] to the imaginary axis on Smith Chart. Some examples will be considered later to show the applicability of the matching and coupling decomposition methods. Take a symmetrical four degree coupling matrix as an example to illustrate the application of the "1" coupling matching, where the coupling matrix is expressed as

$$\bar{A} = \begin{bmatrix} -j & M_{S1} & 0 & 0 & 0 & 0 \\ M_{S1} & p & M_{12} & 0 & 0 & 0 \\ 0 & M_{12} & p & M_{23} & 0 & 0 \\ 0 & 0 & M_{23} & p & M_{34} & 0 \\ 0 & 0 & 0 & M_{34} & p & M_{4L} \\ 0 & 0 & 0 & 0 & M_{4L} & -j \end{bmatrix} \tag{31}$$

where $M_{S1} = M_{4L} = 1.1055$, $M_{12} = M_{34} = 0.9860$, and $M_{23} = 0.7410$. The central frequency of the filter designed is chosen as 10.48 GHz, and

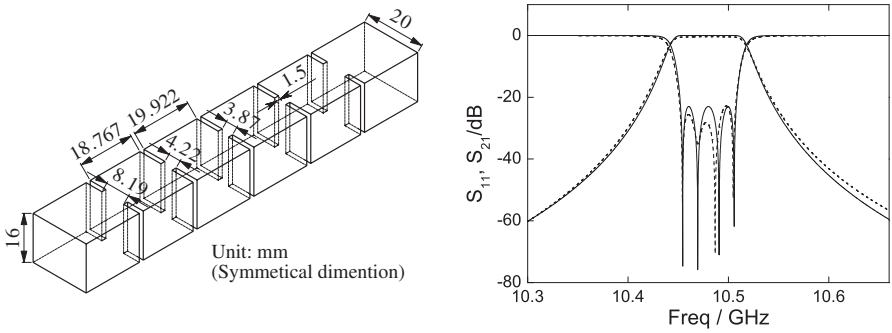

(a) Physical geometry (b) Frequency response

Figure 5. Physical configuration and frequency response of the filter. Solid line: Ideal response; Dashed line: Simulated response.

the equal-ripple bandwidth is 55.5 MHz.

Figure 5 shows the model and response of the waveguide filter. The ideal responses are calculated using MatLab software package, and the simulated results are calculated using the commercial microwave software HFSS.

5. SPECIFIC APPLICATIONS

By taking reference to the transformation of (23), the filter responses corresponding to the coupling matrix of (31) and $\bar{B}$ shown in (32) are the same.

$$\bar{B} = \begin{bmatrix} -j & M_{S1} & 0 & 0 & 0 & 0 & 0 & 0 \\ M_{S1} & p & M_{12} & 0 & 0 & 0 & 0 & 0 \\ 0 & M_{12} & p & \sqrt{M_{23}} & 0 & 0 & 0 & 0 \\ 0 & 0 & \sqrt{M_{23}} & 0 & 1 & 0 & 0 & 0 \\ 0 & 0 & 0 & 1 & 0 & -\sqrt{M_{23}} & 0 & 0 \\ 0 & 0 & 0 & 0 & -\sqrt{M_{23}} & p & M_{34} & 0 \\ 0 & 0 & 0 & 0 & 0 & M_{34} & p & M_{4L} \\ 0 & 0 & 0 & 0 & 0 & 0 & M_{4L} & -j \end{bmatrix} \tag{32}$$

Additionally, (32) can be decomposed to the following two sub-matrices

$$A_1 = \begin{bmatrix} -j & M_{S1} & 0 & 0 \\ M_{S1} & p & M_{12} & 0 \\ 0 & M_{12} & p & \sqrt{M_{23}} \\ 0 & 0 & \sqrt{M_{23}} & -j \end{bmatrix} \tag{33}$$

$$A_2 = \begin{bmatrix} -j & \sqrt{M_{23}} & 0 & 0 \\ \sqrt{M_{23}} & p & M_{34} & 0 \\ 0 & M_{34} & p & M_{4L} \\ 0 & 0 & M_{4L} & -j \end{bmatrix}. \tag{34}$$

From (25), (26) and (27), the ideal filter responses corresponding to coupling matrices $\bar{A}$ in (31) and cascade connected coupling matrices (33) and (34) are equivalent. The two sub-matrices have the same ideal responses which are compared and shown in Fig. 6.

We can use a transmission line to achieve the "1" coupling matching section. Changing the output waveguide length L, we can obtain the responses of reflection to the sub-filters, which are plotted in Fig. 7 using the smith chart.

When the reflection chart of every sub-filter is perpendicular to the real axis of the smith chart, and their phase difference is π,

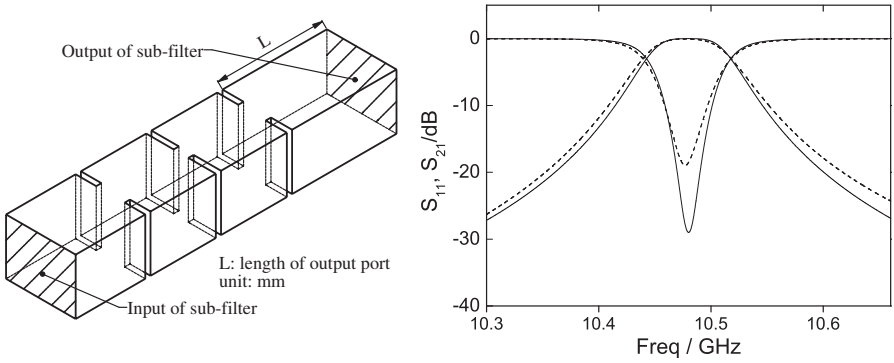

Figure 6. Ideal (solid line) and simulated (dashed line) responses used for the sub-filters.

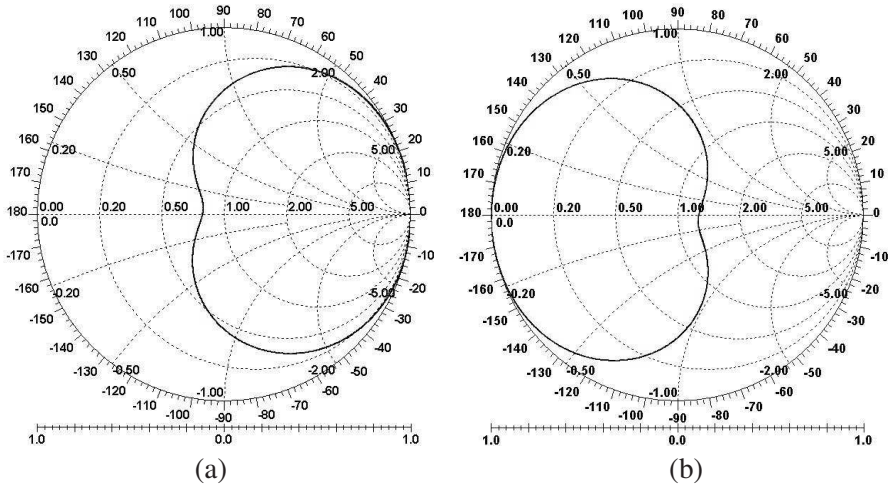

Figure 7. The port-reflection-coefficient smith charts of sub-filters in Fig. 6 by changing the input waveguide length L: (a) $L = 8.7\,\text{mm}$, (b) $L = 18.9\,\text{mm}$.

then the approximate conjugate matching of the two sub-filters is realized in the passband. As a result, the length of the transmission line corresponding to the NRN matching is 27.6 mm, the length is about $\lambda_g\,(\phi_1 + \phi_2 + \pi/4)$ [at the center frequency of the pass-band, $\lambda_g = 40.98\,\text{mm}$]. In the first chart of Fig. 7, $L_1 = 8.7\,\text{mm}$; and in the second chart, $L_2 = 18.9\,\text{mm}$, the difference of L_1 and L_2 is about one quarter waveguide wavelength.

The physical model depicted in Fig. 8 is the filter combined with the two sub-filters, whose responses are shown in Fig. 7. The second figure shown is its response chart.

The NRN waveguide transmission lines can be substituted with coaxial transmission lines, the dielectric constant is $\varepsilon_r = 2.08$. The reflection coefficient tracks of the two sub-filters are shown in Fig. 9.

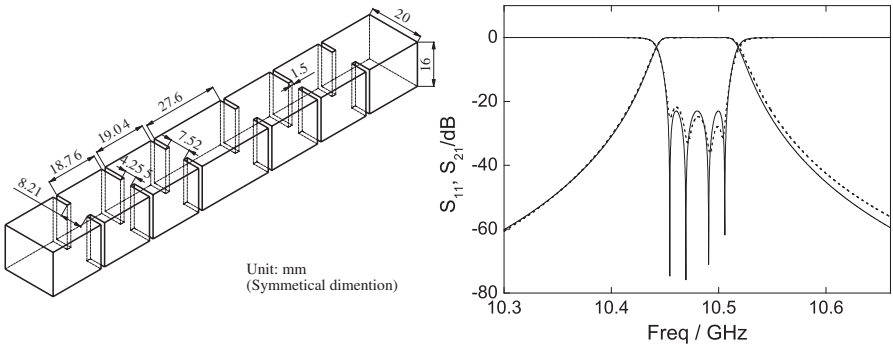

(a) Physical geometry (b) Frequency response

Figure 8. Physical configuration and frequency response of the filter with NRN section, solid line: ideal response; dashed line: simulated response.

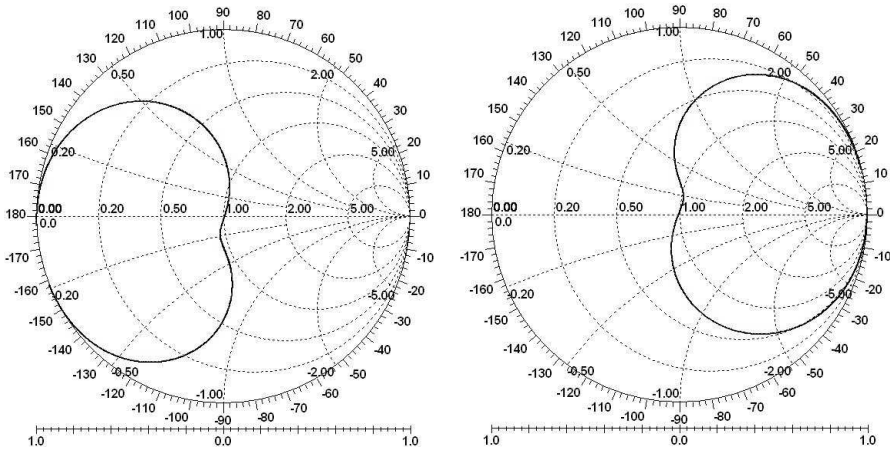

(a) (b)

Figure 9. Frequency responses of two coaxial transmission lines. The lengths of the coaxial lines are (a) 3.55 mm and (b) 8.6 mm, respectively.

The response of the filter, after combination, is shown in Fig. 10(b). The length of the transmission coaxial line is 12.01 mm, and the physical model or geometry of the filter is also shown in Fig. 10(a).

In order to investigate the influence of the NRN structures, simulated wideband responses are compared in Fig. 11, from which, filters using coaxial-line or waveguide as NRN structures have similar responses in a wide frequency band from 8 GHz to 10 GHz. However, in frequency band below 9.5 GHz or above 11.5 GHz, the ideal insertion loss of the filters using NRN structures is about 40 dB higher than that of the original response, because the NRN resonates in outband.

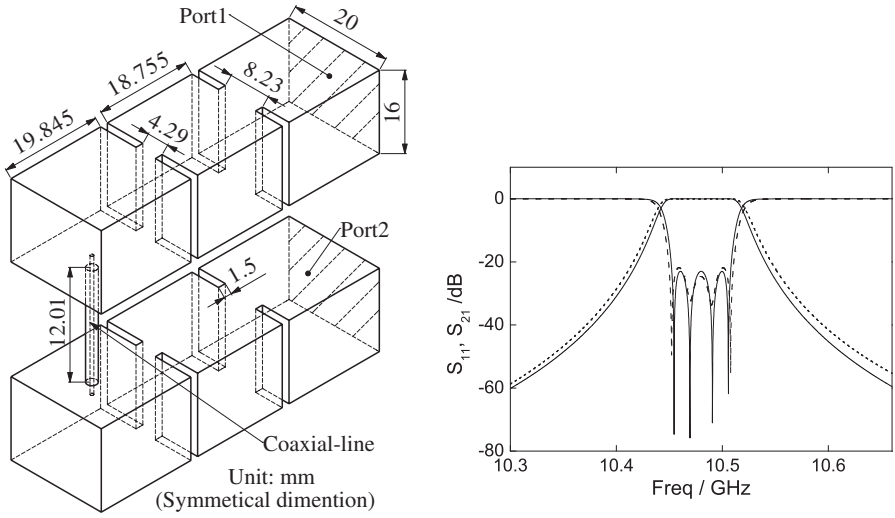

(a) Physical geometry (b) Frequency response

Figure 10. Physical configuration and response of the filter with NRN coaxial connection.

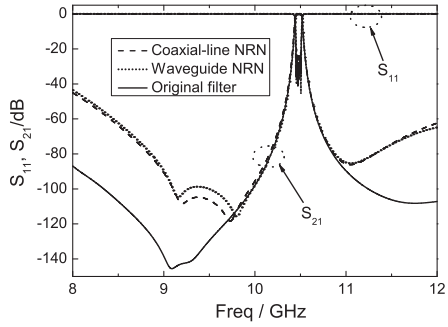

Figure 11. Compared results of wideband responses.

6. CONCLUSION

The decomposition of the coupling coefficients is proposed and carried out in this paper so as to decompose the coupling matrix to multiple sub-matrices. The physical significance of NRN coupling is then analyzed using the conjugated matching method, and the original filter can be decomposed into many sub-filters. The method proposed in the paper can be used to make coupling values more physically realizable, although it may cause a more flexible topology. It is obvious that by increasing the length of NRN coupling coaxial line by $n\lambda_g/2$, the response of the filter does not change. This is an important feature and may lead to many potential applications in the filter designs.

REFERENCES

1. Ragan, G. L., *Microwave Transmission Circuits*, McGraw Hill, New York, 1948.
2. Mo, S. G., Z. Y. Yu, and L. Zhang, "Design of triple-mode bandpass filter using improved hexagonal loop resonator," *Progress In Electromagntics Research*, Vol. 96, 117–125, 2009.
3. Wen, S. and L. Zhu, "Numerical synthesis design of coupled resonator filters," *Progress In Electromagntics Research*, Vol. 92, 333–346, 2009.
4. Hejazi, Z. M., M. C. Scardelletti, F. W. Van Keuls, A. A. Omar, and A. S. Al-Zayed, "EM full-wave analysis and testing of novel quasi-elliptic microstrip filters for ultra narrowband filter design," *Progress In Electromagntics Research*, Vol. 85, 261–288, 2008.
5. Kung, C. Y., Y. C. Chen, S. M. Wu, C. F. Yang, and J. S. Sun, "A novel compact 2.4/5.2 GHz dual wideband bandpass filter with deep transmission zero," *Journal of Electromagnetic Waves and Applications*, Vol. 25, No. 5–6, 617–628, 2011.
6. Naghshvarianjahromi, M., "Novel compact meta-material tunable Quasi elliptic band-pass filter using microstrip to slotline transition," *Journal of Electromagnetic Waves and Applications*, Vol. 24, No. 17–18, 2371–2382, 2010.
7. Cogollos, S., R. J. Cameron, R. R. Mansour, M. Yu, and V. E. Boria, "Synthesis and design procedure for high performance waveguide filters based on nonresonating nodes," *IEEE MTT-S International Microwave Symposium Digest*, 1297–1300, 2007.
8. Zhu, Y. Z., Song, H. S. and Guan, K., "Design of optimized selective quasi-elliptic filters," *Journal of Electromagnetic Waves and Applications*, Vol. 23, No. 10, 1357–1366, 2009.

9. Zhang, L., Z. Y. Yu, and L. Guo, "Compact planar triple-mode bandpass filter with enhanced parasitic coupling," *Journal of Electromagnetic Waves and Applications*, Vol. 24, No. 4, 495–503, 2010.
10. Li, R. Q., X. H. Tang, and F. Xiao, "An novel substrate integrated waveguide square cavity dual-mode filter," *Journal of Electromagnetic Waves and Applications*, Vol. 23, No. 4, 2523–2529, 2009.
11. Hu, G., C. Liu, L. Yan, K. Huang, and W. Menzel, "Novel dual mode substrate integrated waveguide band-pass filters," *Journal of Electromagnetic Waves and Applications*, Vol. 24, No. 11–12, 1661–1672, 2010.
12. Shen. W., Yin, W. Y. and Sun, X. W., "Compact substrate integrated waveguide transversal filter with microstrip dual-mode resonator," *Journal of Electromagnetic Waves and Applications*, Vol. 24, Nos. 14–15, 1887–1896, 2010.
13. Amari, S. and U. Rosenberg, "New building blocks for modular design of elliptic and self-equalized filters," *IEEE Tran. Microwave Theory Tech.*, Vol. 52, 721–736, 2004.
14. Li, R. Q., X. H. Tang, and F. Xiao, "Design of substrate integrated waveguide filters with source/load-multiresonator coupling," *Journal of Electromagnetic Waves and Applications*, Vol. 24, No. 14–15, 1967–1975, 2010.
15. Chu, Q. X. and L. Fan, "A compact bandpass filter with source-load coupling by using short-circuited coupled lines between ports," *Journal of Electromagnetic Waves and Applications*, Vol. 24, No. 11–12, 1493–1500, 2010.
16. Hong, J. S. and M. J. Lancaster, *Microstrip Filters for RF/Microwave Applications*, John Wiley, Inc., 2001.